# Stimulus relevance modulates contrast adaptation in visual cortex

Keller, Andreas J ; Houlton, Rachael ; Kampa, Björn M ; Lesica, Nicholas A ; Mrsic-Flogel, Thomas D ; Keller, Georg B ; Helmchen, Fritjof

DOI: https://doi.org/10.7554/eLife.21589

# Stimulus relevance modulates contrast adaptation in visual cortex

Andreas J. Keller[1,2,3,*], Rachael Houlton[4], Björn M. Kampa[2,7], Nicholas A. Lesica[6], Thomas D. Mrsic-Flogel[4,5], Georg B. Keller[3,8], Fritjof Helmchen[2,8]

[1] *Institute of Neuroinformatics, University of Zurich and ETH Zurich Winterthurerstrasse 190, CH-8057 Zurich, Switzerland*

[2] *Brain Research Institute, University of Zurich, Winterthurerstrasse 190, CH-8057 Zurich, Switzerland*

[3] *Friedrich Miescher Institute for Biomedical Research, Maulbeerstrasse 66, CH-4058 Basel, Switzerland*

[4] *Department of Neuroscience, Physiology and Pharmacology, University College London, 21 University Street, London WC1E 6DE, United Kingdom*

[5] *Biozentrum, University of Basel, Klingelbergstrasse 50/70, CH-4056 Basel, Switzerland*

[6] *Ear Institute, University College London, London WC1E 6BT, United Kingdom*

[7] *Department of Neurophysiology, Institute of Biology 2, RWTH Aachen University, Aachen, Germany*

[8] *Co-senior author*

[*]Correspondence: andi@ini.ethz.ch (A.J.K.)

**A general principle of sensory processing is that neurons adapt to sustained stimuli by reducing their response over time. Most of our knowledge on adaptation in single cells is based on experiments in anesthetized animals. How responses adapt in awake animals, when stimuli may be behaviorally relevant or not, remains unclear. Here we show that contrast adaptation in mouse primary visual cortex depends on the behavioral relevance of the stimulus. Cells that adapted to contrast under anesthesia maintained or even increased their activity in awake naïve mice. When engaged in a visually guided task, contrast adaptation re-occurred for stimuli that were irrelevant for solving the task. However, contrast adaptation was reversed when stimuli acquired behavioral relevance. Regulation of cortical adaptation by task demand may allow dynamic control of sensory-evoked signal flow in the neocortex.**

Our sensory systems constantly receive streams of sensory signals. The computational resources to process this input, however, are limited. Neural circuits in sensory systems have been shown to reduce responses to sustained stimuli (Adrian and Zotterman 1926; Albrecht, Farrar, and Hamilton 1984; Maffei, Fiorentini, and Bisti 1973) or selectively enhance aspects of the sensory input that are relevant to a behavioral task (Desimone and Duncan 1995; Ito and Gilbert 1999; Kato, Gillet, and Isaacson 2015; Reynolds and Heeger 2009; Zhang et al. 2014). In visual cortex, neural responses to a sustained stimulus adapt over the course of a few seconds. Thus, a proposed function of adaptation is to redistribute processing resources to behaviorally relevant or novel stimuli. Most experiments on adaptation, however, were carried out in anesthetized animals. While sensory-evoked responses are known to be modulated by task engagement or

attention (Ito and Gilbert 1999; Harris and Mrsic-Flogel 2013; Reynolds and Chelazzi 2004), it is still unclear if cortical adaptation is modulated by the behavioral relevance of the stimulus.

To test the behavioral dependence of cortical response adaptation, we presented sustained moving grating stimuli to mice in different behavioral states and in conditions with different behavioral relevance of the visual test stimulus. Consistent with previous findings (Ahmed et al. 1997; Carandini and Ferster 1997; Sanchez-Vives, Nowak, and McCormick 2000; Vidyasagar 1990; A. J. Keller and Martin 2015), we found that the responses of neurons in anaesthetized mouse primary visual cortex (V1) adapt to sustained high-contrast grating stimuli (**Figure 1**), and that this adaptation depends on local cortical activity (King et al. 2016) (**Figure 1-figure supplement 1**). Several mechanisms have been proposed to underlie such contrast adaptation (Ahmed et al. 1997; Carandini and Ferster 1997; Sanchez-Vives, Nowak, and McCormick 2000; Vidyasagar 1990; A. J. Keller and Martin 2015), including tonic feedforward inhibition mediated by parvalbumin positive (PV+) interneurons (Ahmed et al. 1997; A. J. Keller and Martin 2015). Accordingly, we found that PV+ neurons adapt less than putative excitatory neurons and that adaptation is only weakly orientation-specific for both neuron types (**Figure 1-figure supplement 2**). To test if neural responses also adapt in awake mice, we compared adaptation measured in the same neurons using two-photon calcium imaging under anesthesia and during wakefulness. As opposed to data obtained under anesthesia, we found that adaptation was absent and neural activity even increased during sustained grating presentations in awake recordings (**Figure 1** and **Figure 1-figure supplements 2i-l,3,4**). Adaptation was stronger (i.e. slope of adaptation more negative) for almost all cells in anesthetized compared to awake mice (**Figure 1-figure supplement 3a**). This reversal of adaptation in awake mice could be explained neither

by response saturation, nor locomotion, nor eye movements (**Figure 1d** and **Figure 1-figure supplements 2i,k,3**). We hypothesize that an attentional mechanism could prevent adaptation when a stimulus is of unknown relevance to the animal. If so, adaptation should reappear if mice divert attention away from the stimulus and learn that the stimulus is behaviorally irrelevant.

To test the role of stimulus relevance for adaptation, we designed a simple visual navigation task (**Figure 2**), in which mice were trained to run to reach the end of a virtual tunnel using visual feedback, while a drifting grating was presented in a fixed part of the visual field (probe patch, centered on the retinotopic location of the recording site; see Materials and methods). Consistent with the lack of adaptation in the passively observing awake mouse (**Figure 1**), we found that adaptation to the grating stimulus was absent initially. As mice learned to perform the navigation task, however, adaptation of neural responses to the grating stimulus reappeared ('grating-irrelevant' condition, **Figure 2e,g,h, Figure 2-figure supplement 1a, Video 1**). This reappearance of adaptation suggests that mice, as they learned to interact with the task-relevant part of the visual field, diverted attention away from the grating stimulus that contained no task-relevant information. Based on this finding, we predicted that for an identical visual input, but when the grating stimulus is behaviorally relevant, neural responses should not adapt with experience. To test this prediction, we showed a different group of mice a replay of the visual stimulus sequence generated by one of the mice in the grating-irrelevant group but increased the behavioral relevance of the grating stimuli by delivering a water reward at the offset of the grating ('grating-relevant' condition, **Figure 2f-h, Figure 2-figure supplement 1b**). We found that adaptation remained absent over training sessions in the grating-relevant group, despite visual experience being identical to the grating-irrelevant group. Moreover, when mice exhibited

anticipatory licking to the reward, neural responses showed an effect opposite to adaptation and activity increased over the course of the stimulus presentation (**Figure 2-figure supplement 2a-i**). We verified that the differences in adaptation between the grating-relevant group and the grating-irrelevant group cannot be explained by learning-related changes in mean running speed, time spent running or number of saccades (**Figure 2-figure supplement 2j-l**). These results suggest therefore that in behaving animals contrast adaptation is modulated bidirectionally by stimulus relevance (**Figure 2-figure supplement 2f,i**).

Thus, the responses of neurons in layer 2/3 of V1 do not adapt to sustained stimuli that are behaviorally relevant, but they do adapt if the stimulus within their receptive field is irrelevant and animals learn to direct attention away from it to other parts of the visual field. These effects are likely mediated by attentional mechanisms (Zhang et al. 2014; Kim et al. 2016) that could directly enhance the responses to relevant stimuli to prevent adaptation. The attentional modulation of adaptation was also not simply explained by changes in adaptation of inhibitory neurons (data not shown) and is unlikely to be generated only locally.

In contrast to our findings on in mouse V1, fMRI studies on awake humans have found response adaptation in V1 upon the presentation of visual patterns (Gardner et al. 2005; Fang et al. 2005; Huk and Heeger 2001, but see Kastner et al. 2003). This disparity is likely the result of small but relevant differences in study design. For example, Huk and Heeger (2001) find a weak adaptation in V1 when participants were attending to two separate moving plaid stimuli. This could be explained by the fact that distributing attention decreases attentional effects (Ito and Gilbert 1999). Other studies (Gardner et al. 2005; Fang et al. 2005) used stimuli that are known to cause adaptation in thalamus and even the retina (Smirnakis et al. 1997; Chander and

Chichilnisky 2001) and cannot distinguish the effects of cortical adaptation from those of subcortical adaptation.

In summary, we have shown that adaptation is dynamically regulated by task demand during learning. Our data are consistent with the idea that cortex dynamically regulates the flow of sensory information by suppressing responses to non-relevant stimuli through mechanisms of adaptation, while boosting sensory responses that are behaviorally important.

## MATERIALS AND METHODS

### Animals

All experiments and surgical procedures were carried out in accordance with the UK Animal (Scientific Procedures) Act under project license 70/7573, approved by the Cantonal Veterinary Office of Zurich, Switzerland, under license number 62/2011, or by the Cantonal Veterinary Office of Basel-Stadt, Switzerland, under license number 2537.

For the electrophysiology experiments, we used transgenic mice selectively expressing channelrhodopsin-2 in parvalbumin-positive neurons (PV+). These mice were generated by crossing *Pvalb*$^{Cre}$ (Jackson 008069) and *Ai32* animals (Jackson 012569). Data were collected from 6 mice (2 female, 4 male, P39-P83).

For the two-photon experiments on mice not engaged in visually-guided behavior, we used transgenic mice selectively expressing tdTomato in PV+ neurons. These mice were generated by

crossing *Pvalb*$^{Cre}$ mice (Jackson 008069) with the *Ai14* reporter line (Jackson 007914). Data were collected from 8 adult mice (2 female, 6 male, P90-161).

For the two-photon experiments on mice engaged in visually-guided behavior (grating-irrelevant and grating-relevant condition), we used transgenic mice selectively expressing tdTomato in GABAergic neurons. These mice were generated by crossing *Slc32a1*$^{Cre}$ mice (Jackson 016962) with the *Ai9* reporter line (Jackson 007909). Data were collected from 7 mice (2 female, 5 male, P80-P282) for the grating-irrelevant condition and 6 mice (1 female, 5 male, P80-P286) for the grating-relevant condition.

**Surgical procedures and anesthesia**

For the electrophysiology experiments, animals were anesthetized with a mixture of Fentanyl (Sublimaze, 0.05 µg/g of body weight), Midazolam (5.0 µg/g of body weight) and Medetomidim (Domitor, 0.5 µg/g of body weight) injected intraperitoneal (i.p.). An adequate depth of anesthesia was indicated by lack of response to toe pinch. Eye cream (Isoptomax) was applied to the eyes to prevent dehydration during surgery. Atropine Sulphate (Hameln Pharmaceuticals, 0.02 µg/g of body weight) and Dexamethasone Sodium Phosphate (Hospira, 0.8 µg/g of body weight) were injected subcutaneously to reduce secretions and edema, respectively. Cortex buffer solution (125 mM NaCl, 5 mM KCl, 10 mM glucose, 10 mM HEPES, 2 mM $MgSO_4$, and 2 mM $CaCl_2$ [pH 7.4], 50 µl) was also injected subcutaneously to prevent dehydration. Throughout the experiment, body temperature was maintained at 38°C, measured with a rectal probe and controlled with a heating blanket. Fur was trimmed and an incision was made at the rear of the head, approximately level with the ears. The skull was cleared of tissue and

immobilized by affixing it to a metal head plate using dental cement (Paladur, Heraeus Kulzer). The plate was then secured in a frame with the head in a horizontal position. A small craniotomy (~2 mm diameter) was made above the right monocular primary visual cortex (V1), determined by stereotaxic coordinates, using a high-speed foot-operated drill (Foredom). The exposed cortical surface was kept moist with cortex buffer solution (see above). The dura was removed and the cortex was covered with 2% agarose following initial electrode array insertion. After surgery, the eye cream was removed except for a thin layer, keeping the eye moist whilst minimizing any visual disturbance.

For the two-photon experiments on mice not engaged in visually-guided behavior, the implantation of the hook for head fixation and the virus injection were performed in two separate surgeries. First, the animals were anesthetized with isoflurane (1-2%). Throughout the surgery, body temperature was measured and controlled with a heating pad. An eye cream (Vitamine A, Bausch&Lomb) and a local anesthetic (Xylocain Gel 2%, AstraZeneca) were applied. Atropine (0.3 µg/g of body weight) and dexamethasone (2 µg/g of body weight) were injected subcutaneously. The skull was cleared and a bonding agent (iBOND Total Etch, Heraeus Kulzer) applied. A hook for head fixation was implanted by first applying a droplet of super-glue (Ultra Gel, Pattex). The hook was fixated using light curable dental cement (Tetric EvoFlow, ivoclar vivadent). Betadine was applied to the wound. Antibiotics (100 µg/g of body weight, ceftriaxone, Rocephin, Roche) and pain killers (5 µg/g of body weight, Metacam, Boehringer Ingelheim) were injected subcutaneously before animals woke up. In the second surgery, the skull was thinned above the right monocular visual cortex, determined by stereotaxic coordinates. The eye cream was carefully removed and optical intrinsic imaging was performed to map V1 (see

below). After making a craniotomy (3 or 4 mm diameter), 2-3 injections of 150 nl of AAV2/1-*hsyn*-GCaMP6m were made based on the intrinsic imaging and a glass coverslip was positioned. Each experiment consisted of an awake followed by an anesthetized part. For the latter we used isoflurane (0.4-1%). Throughout the anesthetized part, body temperature was measured and maintained at 38°C with a heating pad.

For the two-photon experiments on mice engaged in visually-guided behavior (grating-irrelevant and grating-relevant condition), surgical procedures have been described elsewhere (Leinweber et al. 2014). Briefly, the animals were anesthetized with an i.p. injection of a mixture of Fentanyl (Sublimaze, 0.05 µg/g of body weight), Midazolam (5.0 µg/g of body weight) and Medetomidim (Domitor, 0.5 µg/g of body weight). A craniotomy was made over the right monocular V1, determined by stereotaxic coordinates. The mice were injected with 5 injections of 100-200 nl of AAV2/1-*ef1α*-GCaMP6f, before the coverslip was positioned. Finally, a head plate was implanted.

**Electrophysiological recordings and optogenetic stimulation**

Extracellular recordings were made using a multi-tetrode array (Neuronexus, A4x2-tet-5mm-150-200-121) that was perpendicularly inserted into the brain with a computer controlled micromanipulator (Scientifica). The probe consisted of 4 evenly spaced shanks, spanning 600 µm of visual cortex in a medial-lateral plane. Each shank contained 8 electrode sites, split between two tetrode configurations that were separated by a vertical distance of 150 µm. A reference electrode was also inserted into the cortex, away from the recording site, via a separate craniotomy. In order to target superficial cortical layers, the array was slowly lowered until

visually responsive neurons were first encountered. Visual responsiveness was assessed online from multi-unit PSTHs obtained during full-field flash stimuli. Signals were digitized at a sampling frequency of 25 kHz (Tucker Davis Technologies, RZ2 Bioamp processor). For the optogenetic stimulation of the PV+ cells, illumination (470 nm) was provided by a high-power LED light source (Thorlabs), and directed via a fiber optic cable (400 μm, Thorlabs) which was positioned 3-4 mm from the surface of the cortex, where it dispersed to cover an area approximately 3 mm in diameter. LED illumination was kept constant except for the last 500 ms, where the intensity instantaneously reduced to 50% and then linearly decreased to zero to avoid rebound activation (Chuong et al. 2014).

**Intrinsic signal optical imaging**

For the experiments on mice not engaged in visually-guided behavior, optical imaging of intrinsic signals was performed before the virus injection of the calcium indicator. Anesthetized mice were placed in front of a monitor and the cortical surface was illuminated with a 630 nm LED light (Thorlabs). The angle of the monitor was ~45° with respect to the craniocaudal axis of the mice with a distance of 20 cm between the center of the screen and the left eye of the mice. The position of the monitor with respect to the mice was kept constant in the following two-photon experiments. In a circular region with a diameter of 10° in the center of the monitor, a square-wave grating was presented for 5 s. Reflectance images were collected through a 4x objective (Olympus) with a CCD camera (Toshiba TELI CS3960DCL). Intrinsic signal changes were analyzed as fractional reflectance changes relative to the prestimulus average. Injections of the calcium indicator were made based on the intrinsic signals.

## Two-photon calcium imaging

For the experiments on mice not engaged in visually-guided behavior, fluorescence was measured with a custom-built two-photon microscope controlled by HelioScan (www.helioscan.org) (Langer et al. 2013). The scanhead was based on an 8 kHz resonant scanner (Cambridge Technology), used in bidirectional mode. Images were acquired at 77.7 Hz with a resolution of 200 by 200 pixels. Illumination light source was a Ti:sapphire laser (MaiTai HP, Newport Spectra Physics). The excitation wavelength was set to 940 nm or 960 nm. Laser power under the objective (Nikon 16x 0.8 NA) never exceeded 50 mW (laser pulse width ≤ 100 fs at a repetition rate of 80 MHz). A volume stack was acquired at every imaging site.

For the two-photon experiments on mice engaged in visually-guided behavior (grating-irrelevant and grating-relevant condition), fluorescence was measured with a custom-built two-photon microscope (https://sourceforge.net/projects/iris-scanning/) (Leinweber et al. 2014). The scanhead was based on an 8 kHz resonant scanner (Cambridge Technology), used in bidirectional mode. This enabled frame rates of 40 Hz at 400 by 600 pixels. A high-power objective z-piezo stage (Physik Instrumente) was used to move the objective down in steps of approximately 20 μm between frames and return to the initial position after four frames. With this system, we acquired data at four different depths, reducing the effective frame rate from 40 Hz to 10 Hz. Data were acquired with a 250 MHz digitizer (National Instruments) and pre-processed with a custom programmed (https://sourceforge.net/projects/iris-scanning/) FPGA (National Instruments). Illumination light source was a Ti:sapphire laser with a prechirp unit (MaiTai eHP DS, Newport Spectra Physics). The excitation wavelength was set to 910 nm. Laser

power under the objective (Nikon 16× 0.8 NA) never exceeded 50 mW (pulse width ≤ 70 fs at a repetition rate of 80 MHz).

**Treadmill, eye-tracking and visual stimulation**

For the electrophysiology experiments, visual stimuli were generated using the open-source MATLAB (MathWorks) Psychophysics Toolbox (Brainard 1997). Drifting square-wave gratings (3 Hz, 0.04 cpd, 100% contrast) moving in 8 different directions were presented on an LCD monitor (isoluminant at 82 cd/$m^2$).

Then, responses to stimulus blocks of 7 s were measured. Stimulus blocks were interspersed with 3 s of grey screen. Baseline values were obtained from the 2-s time window before each stimulus. On alternate trials, cortex was optogenetically silenced during the first 3.5 s (see above). The stimuli were presented 5-40 times each.

For the two-photon calcium imaging experiments on mice not engaged in visually-guided behavior, head-restrained mice were placed on a spherical air-supported treadmill (Dombeck et al. 2007), which allowed the mice to run or rest at their whim. Visual stimuli were generated using the open-source MATLAB (MathWorks) toolbox StimServer (Muir and Kampa 2015). Drifting sinusoidal gratings (1.5 Hz, 0.04 cpd, 80% contrast) moving in 8 different directions were presented (2 s grating interleaved with 4 s grey screen) on a LED-backlit monitor (BenQ XL2410T, iso-luminant at 23 cd/$m^2$). The power-source of the LED-backlight was synchronized with the resonant scanner turnaround points (when data are not acquired) to minimize light-leak from the monitor (Leinweber et al. 2014). An iso- and cross-orientation (with an angular difference of 90°) were chosen for the adaptation paradigm. We presented a grating for 10 s at

the iso- or cross-orientation at 50% contrast followed by a grating for 10 s at the iso-orientation at 25% or 100% contrast. This resulted in a total of 4 stimulus conditions which were presented in a pseudo-random order for 13-31 times each. The stimulus conditions were interleaved with an iso-luminant grey screen for at least 10 s. Subsequently, the orientation and contrast adaptation paradigms were repeated under anesthesia (presented 30-48 times each). Throughout all imaging sessions, we measured running speed and eye-movements. Saccades were detected using a CMOS based video camera at 30 Hz (DMK 22BUC03, Imaging Source). Pupil position was computed offline by smoothing and thresholding the images and fitting a circle to the pupil. The filter radius and the image threshold were adapted manually for each experiment. Pupil position was filtered using a median filter. Eye movements were detected automatically by applying an adapted threshold. This method was cross-validated in several experiments using manual detection of eye movements.

For the experiments on mice engaged in visually-guided behavior with feedback coupling (grating-irrelevant condition), we first mapped the toroidal screen onto the cortical surface using intrinsic optical signal imaging. Single horizontal and vertical bars were shown moving over the whole surface of the screen. The treadmill, eye-tracking and visual stimulation have been described previously (Leinweber et al. 2014; Dombeck et al. 2007). Briefly, head-restrained mice ran on a spherical air-supported treadmill. Throughout all imaging sessions, we measured the trajectories of the mice in the tunnel and eye-movements with a CMOS based video camera at 30 Hz (DMK 22BUC03, Imaging Source). Mice were learning to use a part of the visual field to navigate to a target location in a virtual reality environment. Each mouse had five training sessions on consecutive days (sessions were spaced by 16-32h). Starting two days before the first

experimental session, mice were water restricted and given a total of at least 1 ml water daily. Weight of the mice was measured daily before and after the training sessions. Before each session, orientation tuning was measured (4 s grating interleaved with 4 s grey screen). During the training session, movement in the virtual tunnel was coupled to the movements of the mice on the spherical treadmill. Mice were trained to orient and run to the end of the tunnel for a water reward (~10 µl per reward) and were immediately teleported back to the start after passing the end of the tunnel. The difficulty of the task (length of the tunnel) was increased during learning to keep the number of rewards approximately constant (~100 per session). Fraction of time spent running across sessions was kept approximately stable by applying occasional air-puffs. Throughout all imaging sessions, we presented a horizontal sinusoidal moving grating (both directions) at 100% contrast in a circular patch (50 degrees in diameter) centered on the retinotopic location of the recording site (45 degrees to the left from the point of view of the mice). This probe patch took up only about an eighth of the entire field of view of the toroidal screen (approximately 200 degrees horizontally, 90 degrees vertically). Grating presentations in the probe patch lasted 10 s (120-163 repetitions per session) and were interspersed with random intervals of grey (10-20 s). Presentations of the drifting grating were not coupled to the behavior of the mice.

For the grating-relevant condition, we repeated the experiment in a new set of mice with two differences. First, the movement in the tunnel was not coupled to their movement on the treadmill but was an exact replay of the visual stimulation used for a mouse under grating-irrelevant condition. The 6 mice under grating-relevant condition were matched to 6 of the 7

mice under grating-irrelevant condition. Second, the mice were not rewarded at the end of the virtual tunnel but 1 s after the offset of the grating.

The experimental paradigm was chosen to allow us to direct the attention of the mouse either away from or towards the gratings stimulus. One potential concern with a choice of paradigm in which the animal has control of the visual flow feedback in the grating-irrelevant condition is that the difference between predicted and actual visual feedback in the probe patch could result in mismatch response (G. B. Keller, Bonhoeffer, and Hübener 2012). Mismatch responses are confined to spatially localized regions in visual space that align to the visual retinotopy (Zmarz and Keller 2016). For this reason, grating-relevant and grating-irrelevant conditions were designed to have equivalent visual flow mismatch in the retinotopic region of the probe patch. Therefore, any potential influence of mismatch responses is equivalent in both conditions. Moreover, neurons are either mismatch responsive, visually driven, or driven by a combination of both (Zmarz and Keller 2016). The neurons we select for in our analysis are the most visually responsive neurons and hence are unlikely to respond to mismatch (Zmarz and Keller 2016).

**Analysis of electrophysiological data**

Electrophysiological data were processed using Matlab (Math-Works) using custom-written code. Single unit spikes were isolated. To this end, channels were bandpass filtered between 500 Hz and 5000 Hz and tetrodes were whitened. We identified potential spikes using an action potential detector described elsewhere (Choi, Jung, and Kim 2006). Then, we performed a principle component analysis (PCA) for each channel using the open-source cluster analysis program KlustaKwik (http://klusta-team.github.io/klustakwik/) (Kadir, Goodman, and Harris

2014). Clusters of potential spikes were determined based on the first three components of the PCA. We calculated the isolation distance of each cluster (Schmitzer-Torbert et al. 2005) and excluded clusters with an isolation distance below 20. The number of potential spikes in the poorly isolated multi-unit activity for each tetrode was always at least as large as the number of spikes in any single-unit cluster. Spike times were determined with a 1 ms resolution.

The preferred stimuli and cell types were determined using the average responses over the first 3.5 s of visual stimulation (see Treadmill, eye-tracking and visual stimulation). For each neuron (total 210 cells), we determined the preferred cardinal orientation. Cells were excluded if they failed to respond in at least half of the trials of their preferred cardinal orientation. Then, we compared the average responses to their preferred cardinal orientation in presence and absence of the optogenetic stimulation. Cells that had a higher average response during optogenetic stimulation were classified as PV+ cells and putative excitatory cells otherwise (data not shown).

All traces of spike rates were binned (~333 ms). Slopes of adaptation (**Figure 1-figure supplement 2a,b**) were estimated by performing a linear regression over 7 s of visual stimulation after normalizing.

**Analysis of two-photon calcium imaging data**

Two-photon calcium images were processed using custom written MATLAB (Math-Works) software.

For the experiments on mice not engaged in visually-guided behavior, we used the open-source toolbox FocusStack (https://bitbucket.org/DylanMuir/twophotonanalysis) (Muir and Kampa 2015). Cells were manually selected using ImageJ (National Institute of Mental Health, NIH).

All traces were filtered using a sliding block filter (20 data points corresponding to ~0.26 s). Fluorescence changes ($\Delta F/F$) were calculated as $(F-F_0)/F_0$ using a 2-s baseline before the stimulus to determine $F_0$. To determine orientation tuning curves, responses were calculated as averages over the whole 2-s presentation of visual stimulus. Preferred orientations were determined by fitting a sum-of-Gaussians to single-cell tuning curves. The Gaussians were forced to peak 180° apart and to have the same tuning width. Cells were classified as tuned to the iso- or cross-orientation (see Treadmill, eye-tracking and visual stimulation) depending on which was closer to the peak of the Gaussian fit. Cells were classified as responsive if in at least 50% of the trials the responses to the preferred orientation (iso- or cross-orientation) were significantly above baseline (Z score > 2.58 corresponding to $p < 0.01$). Fluorescence changes ($\Delta F/F$) for contrast tuning were calculated using a 3-s baseline before the stimulus.

Slopes of adaptation of tuned cells in **Figure 1-figure supplement 2c,d** were estimated by performing a linear regression over 1-7 s of visual stimulation after normalizing. The initial rise (approximated by 1 s) was excluded from the fit. Adaptation in awake and anesthetized mice (**Figure 1** and **Figure 1-figure supplement 3**) was compared using neurons tuned in both states. Slopes of adaptation in **Figure 1d** were estimated by performing a linear regression over 1-9.75 s of visual stimulation (9.75-10 s was excluded due to filtering). Trials were classified as "running" if at least during half the visual stimulation the running speed of the mice exceeded 1 cm/s and "resting" otherwise. Trials were classified as "eye movement" trials if the mice made at least one saccade during the visual stimulation and "eye movement-free" otherwise. Cross- and iso-orientation adaptation in anesthetized and awake mice were compared using neurons that

were tuned in anesthetized or awake mice, respectively (in **Figure 1-figure supplement 2e-h** and **Figure 1-figure supplement 2i-l**, respectively).

For the experiments on mice engaged in visually-guided behavior (grating-irrelevant and grating-relevant condition), analysis of functional imaging data was conducted as described previously (G. B. Keller, Bonhoeffer, and Hübener 2012). Briefly, data were full-frame registered using a custom written software (https://sourceforge.net/projects/iris-scanning/). Cells were selected manually based on mean and maximum projections. Raw fluorescence traces were calculated as the average fluorescence of all pixels within a selected region for each frame. To calculate the fluorescence changes ($\Delta F/F$), the 8-percentile value of the fluorescence distribution in a ±15 s window was subtracted from the raw fluorescence signal, which was then divided by the median of each cell's fluorescence distribution (Dombeck et al. 2007). Responses were calculated as averages over the whole 4-s presentation time of visual stimulus. Preferred orientations were determined by fitting a sum-of-Gaussians to single-cell tuning curves averaged over all sessions. Gaussians were fixed to peak 180° apart and to have the same tuning widths. Cells were classified as tuned to the horizontal grating if the peak of the Gaussian fit was within horizontal ±45°. For all activity traces in **Figure 2** and **Figure 2-figure supplement 2**, average activity during a pre-stimulus baseline of 2 s was subtracted. Cells were classified as responsive if in at least half of the sessions the average responses to the horizontal grating were significantly above or below baseline ($|Z\ score| > 3.29$ corresponding to $p < 0.001$). To match the initial conditions of the grating-relevant and grating-irrelevant conditions, 10% of the neurons in the grating-relevant, reward anticipating and non-anticipating condition were excluded. We excluded cells which in session 1 showed the largest deviations from the mean response in the grating-irrelevant

condition. Note that this did not change the results. The performance was quantified as fraction of time spent running (>1 cm/s) in the direction of the goal with a tolerance of ±25°. Slopes of adaptation and mean responses were estimated by performing a linear regression and averaging over 1-10 s of visual stimulation, respectively (**Figure 2g,h** and **Figure 2-figure supplements 1,2g,h**). To estimate the slopes and means, trial responses were divided into 4 bins per session. Exponential fits were done based on the binned data (4 bins per session).

All lick frequencies were baseline-corrected by subtracting the mean lick frequency 15 s to 13 s before the reward. The pre-reward licking (**Figure 2-figure supplement 2a-c**) was defined as the baseline-corrected lick frequency 0.5 s to 0 s before the reward.


## ACKNOWLEDGEMENTS

This work was supported by EU SECO Grant EU216593, ETH Grant 2-73246-8, and SNF Sinergia to Kevan A. C. Martin, and FP7 EU Grant 269921 ('BrainScaleS') (F.H. and B.M.K), the Novartis Research Foundation (G.B.K.), the Swiss National Science Foundation (G.B.K.), and the European Research Council Grant ('NeuroVision', 616509) and Wellcome Trust Grant 095074 (both to T.D.M-F.). We thank Kevan A. C. Martin for his inestimable support in discussions, funding, and resources. We thank Morgane M. F. Roth for critical comments on the manuscript.

## References


Adrian, E D, and Yngve Zotterman. 1926. “The Impulses Produced by Sensory Nerve Endings. Part 2. The Response of a Single End-Organ.” *J. Physiol.* 61 (2): 151–71. doi:10.1113/jphysiol.1926.sp002281.

Ahmed, Bashir, John D Allison, Rodney J Douglas, and Kevan A C Martin. 1997. “An Intracellular Study of the Contrast-Dependence of Neuronal Activity in Cat Visual Cortex.” *Cereb. Cortex* 7 (6): 559–70. doi:10.1093/cercor/7.6.559.

Albrecht, Duane G, Susan B Farrar, and David B Hamilton. 1984. “Spatial Contrast Adaptation Characteristics of Neurones Recorded in the Cat’s Visual Cortex.” *J. Physiol.* 347: 713–39. doi:10.1113/jphysiol.1984.sp015092.

Atallah, Bassam V, William Bruns, Matteo Carandini, and Massimo Scanziani. 2012. “Parvalbumin-Expressing Interneurons Linearly Transform Cortical Responses to Visual Stimuli.” *Neuron* 73 (1): 159–70. doi:10.1016/j.neuron.2011.12.013.

Brainard, David H. 1997. “The Psychophysics Toolbox.” *Spatial Vision* 10: 433–36. doi:10.1163/156856897X00357.

Carandini, Matteo, and David Ferster. 1997. “A Tonic Hyperpolarization Underlying Contrast Adaptation in Cat Visual Cortex.” *Science* 276 (May): 949–52. doi:10.1126/science.276.5314.949.

Chander, D, and E J Chichilnisky. 2001. “Adaptation to Temporal Contrast in Primate and Salamander Retina.” *The Journal of Neuroscience* 21 (24): 9904–16.

http://www.ncbi.nlm.nih.gov/pubmed/11739598.

Chen, Tsai-Wen, Trevor J. Wardill, Yi Sun, Stefan R. Pulver, Sabine L. Renninger, Amy Baohan, Eric R. Schreiter, et al. 2013. “Ultrasensitive Fluorescent Proteins for Imaging Neuronal Activity.” *Nature* 499 (7458): 295–300. doi:10.1038/nature12354.

Choi, Joon Hwan, Hae Kyung Jung, and Taejeong Kim. 2006. “A New Action Potential Detector Using the MTEO and Its Effects on Spike Sorting Systems at Low Signal-to-Noise Ratios.” *IEEE Transactions on Biomedical Engineering* 53 (4): 738–46. doi:10.1109/TBME.2006.870239.

Chuong, Amy S, Mitra L Miri, Volker Busskamp, Gillian A C Matthews, Leah C Acker, Andreas T Sørensen, Andrew Young, et al. 2014. “Noninvasive Optical Inhibition with a Red-Shifted Microbial Rhodopsin.” *Nature Neuroscience* 17 (8). Nature Publishing Group: 1123–29. doi:10.1038/nn.3752.

Desimone, R, and J Duncan. 1995. “Neural Mechanisms of Selective Visual Attention.” *Annual Review of Neuroscience* 18 (January): 193–222. doi:10.1146/annurev.ne.18.030195.001205.

Dombeck, Daniel A., Anton N. Khabbaz, Forrest Collman, Thomas L. Adelman, and David W. Tank. 2007. “Imaging Large-Scale Neural Activity with Cellular Resolution in Awake, Mobile Mice.” *Neuron* 56 (1): 43–57. doi:10.1016/j.neuron.2007.08.003.

Engel, Stephen A, and Christopher S Furmanski. 2001. “Selective Adaptation to Color Contrast in Human Primary Visual Cortex.” *The Journal of Neuroscience* 21 (11): 3949–54. doi:21/11/3949.

Fang, Fang, Scott O Murray, Daniel Kersten, and Sheng He. 2005. “Orientation-Tuned fMRI Adaptation in Human Visual Cortex.” *J Neurophysiol* 94 (6): 4188–95. doi:10.1152/jn.00378.2005.

Gardner, Justin L., Pei Sun, R. Allen Waggoner, Kenichi Ueno, Keiji Tanaka, and Kang Cheng. 2005. “Contrast Adaptation and Representation in Human Early Visual Cortex.” *Neuron* 47 (4): 607–20. doi:10.1016/j.neuron.2005.07.016.

Harris, Kenneth D., and Thomas D. Mrsic-Flogel. 2013. “Cortical Connectivity and Sensory Coding.” *Nature* 503 (7474). Nature Publishing Group: 51–58. doi:10.1038/nature12654.

Hofer, Sonja B, Ho Ko, Bruno Pichler, Joshua Vogelstein, Hana Ros, Hongkui Zeng, Ed Lein, Nicholas A Lesica, and Thomas D Mrsic-Flogel. 2011. “Differential Connectivity and Response Dynamics of Excitatory and Inhibitory Neurons in Visual Cortex.” *Nature Neuroscience* 14 (8): 1045–52. doi:10.1038/nn.2876.

Huk, Alexander C, and David J Heeger. 2001. “Pattern-Motion Responses in Human Visual Cortex.” *Nat.Neurosci.* 5 (1): 72–75. doi:10.1038/nn774.

Ito, M, and C D Gilbert. 1999. “Attention Modulates Contextual Influences in the Primary Visual Cortex of Alert Monkeys.” *Neuron* 22 (3): 593–604. doi:10.1016/S0896-6273(00)80713-8.

Kadir, Shabnam N, Dan F M Goodman, and Kenneth D Harris. 2014. “Neuronal Spike Train Entropy Estimation by History Clustering.” *Neural Computation* 26: 2379–94. doi:10.1162/NECO.

Kastner, Sabine, Daniel H O’Connor, Miki M Fukui, Hilda M Fehd, Uwe Herwig, and Mark A

Pinsk. 2003. “Functional Imaging of the Human Lateral Geniculate Nucleus and Pulvinar.” *J Neurophysiol* 17 (1): 17. doi:10.1152/jn.00553.2003.

Kato, Hiroyuki K., Shea N. Gillet, and Jeffry S. Isaacson. 2015. “Flexible Sensory Representations in Auditory Cortex Driven by Behavioral Relevance.” *Neuron* 88 (5). Elsevier Inc.: 1027–39. doi:10.1016/j.neuron.2015.10.024.

Keller, Andreas J, and Kevan A C Martin. 2015. “Local Circuits for Contrast Normalization and Adaptation Investigated with Two-Photon Imaging in Cat Primary Visual Cortex.” *Journal of Neuroscience* 35 (27): 10078–87. doi:10.1523/JNEUROSCI.0906-15.2015.

Keller, Georg B, Tobias Bonhoeffer, and Mark Hübener. 2012. “Sensorimotor Mismatch Signals in Primary Visual Cortex of the Behaving Mouse.” *Neuron* 74 (5): 809–15. doi:10.1016/j.neuron.2012.03.040.

Kerlin, Aaron M, Mark L Andermann, Vladimir K Berezovskii, and R Clay Reid. 2010. “Broadly Tuned Response Properties of Diverse Inhibitory Neuron Subtypes in Mouse Visual Cortex.” *Neuron* 67 (5). Elsevier Inc.: 858–71. doi:10.1016/j.neuron.2010.08.002.

Kim, Hoseok, A Sofie, Xinming Wang, Karl Deisseroth, Marie Carle, Xinming Wang, Karl Deisseroth, Marie Carle, Hoseok Kim, and A Sofie. 2016. “Prefrontal Parvalbumin Neurons in Control of Article Prefrontal Parvalbumin Neurons in Control of Attention,” 208–18. doi:10.1016/j.cell.2015.11.038.

King, Jillian L, Matthew P Lowe, Kurt R Stover, Aimee A Wong, and Nathan A Crowder. 2016. “Adaptive Processes in Thalamus and Cortex Revealed by Silencing of Primary Visual

Cortex during Contrast Adaptation." *Current Biology*. Elsevier Ltd, 1–6. doi:10.1016/j.cub.2016.03.018.

Langer, Dominik, Marcel van 't Hoff, Andreas J Keller, Chetan Nagaraja, Oliver A Pfäffli, Maurice Göldi, Hansjörg Kasper, and Fritjof Helmchen. 2013. "HelioScan: A Software Framework for Controlling in Vivo Microscopy Setups with High Hardware Flexibility, Functional Diversity and Extendibility." *J. Neurosci. Meth.* 215 (1). Elsevier B.V.: 38–52. doi:10.1016/j.jneumeth.2013.02.006.

Leinweber, Marcus, Pawel Zmarz, Peter Buchmann, Paul Argast, Mark Hübener, Tobias Bonhoeffer, and Georg B Keller. 2014. "Two-Photon Calcium Imaging in Mice Navigating a Virtual Reality Environment." *Journal of Visualized Experiments : JoVE*, no. 84: e50885. doi:10.3791/50885.

Maffei, L, A Fiorentini, and S Bisti. 1973. "Neural Correlate of Perceptual Adaptation to Gratings." *Science* 182 (December): 1036–38. doi:10.1126/science.182.4116.1036.

Muir, Dylan R, and Björn M Kampa. 2015. "FocusStack and StimServer: A New Open Source MATLAB Toolchain for Visual Stimulation and Analysis of Two-Photon Calcium Neuronal Imaging Data." *Frontiers in Neuroinformatics* 8 (January): 85. doi:10.3389/fninf.2014.00085.

Reynolds, John H., and David J. Heeger. 2009. "The Normalization Model of Attention." *Neuron* 61 (2). Elsevier Inc.: 168–85. doi:10.1016/j.neuron.2009.01.002.

Reynolds, John H, and Leonardo Chelazzi. 2004. "Attentional Modulation of Visual Processing."

499 *Annual Review of Neuroscience* 27 (January): 611–47.
500 doi:10.1146/annurev.neuro.26.041002.131039.

501 Sanchez-Vives, Maria V, Lionel G Nowak, and David A McCormick. 2000. "Membrane
502 Mechanisms Underlying Contrast Adaptation in Cat Area 17 In Vivo." *The Journal of*
503 *Neuroscience* 20 (11): 4267–85.

504 Schmitzer-Torbert, N., J. Jackson, D. Henze, K. Harris, and A. D. Redish. 2005. "Quantitative
505 Measures of Cluster Quality for Use in Extracellular Recordings." *Neuroscience* 131 (1): 1–
506 11. doi:10.1016/j.neuroscience.2004.09.066.

507 Smirnakis, Stelios M, Michael J Berry Ii, David K Warland, William Bialek, and Markus
508 Meister. 1997. "Adaptation of Retinal Processing to Image Contrast and Spatial Scale."
509 *Nature*. doi:10.1038/386069a0.

510 Stroud, Aaron C, Emily E Ledue, and Nathan A Crowder. 2012. "Orientation Specificity of
511 Contrast Adaptation in Mouse Primary Visual Cortex." *Journal of Neurophysiology* 108 (5):
512 1381–91. doi:10.1152/jn.01148.2011.

513 Vidyasagar, T R. 1990. "Pattern Adaptation in Cat Visual Cortex Is a Co-Operative
514 Phenomenon." *Neuroscience* 36 (1): 175–79. doi:10.1016/0306-4522(90)90360-G.

515 Zhang, Siyu, Min Xu, Tsukasa Kamigaki, Johnny Phong Hoang Do, Wei-Cheng Chang, Sean
516 Jenvay, Kazunari Miyamichi, Liqun Luo, and Yang Dan. 2014. "Long-Range and Local
517 Circuits for Top-down Modulation of Visual Cortex Processing." *Science* 345 (6197): 660–
518 66. doi:10.1126/science.1254126.

519 Zmarz, Pawel, and Georg B. Keller. 2016. “Mismatch Receptive Fields in Mouse Visual
520 Cortex.” *Neuron*. Elsevier Inc., 1–7. doi:10.1016/j.neuron.2016.09.057.

521

## FIGURE LEGENDS

**Figure 1** Contrast adaptation in awake and anesthetized mice. **(a)** Schematic of the experimental setup. Calcium imaging with GCaMP6m (Chen et al. 2013) was performed during presentation of drifting sinusoidal gratings. **(b)** Calcium transients from four example putative excitatory cells tuned to a moving sinusoidal grating at 50% contrast (presented for 10 s; grey shadings). The same cells were recorded during wakefulness and anesthesia. **(c)** Averaged calcium responses of tuned putative excitatory cells. Note that even small differences in adaptation can be detected using two-photon imaging (**Figure 1-figure supplement 2a-d**). Curves plotted as mean ± SEM (shading). **(d)** Slope of adaptation of single cells recorded in different behavioral states (same data as in **c**; line fit to the data in time window 1-9.75 s). Anesthetized mice show a significantly more negative slope compared to all other states [anest. (169 cells) – awake (169 cells): $p < 10^{-10}$; Wilcoxon signed-rank; running (51 cells): $p < 10^{-4}$; resting (169 cells): $p < 10^{-10}$; eye movements (168 cells): $p < 10^{-10}$; eye movement-free (165 cells): $p < 10^{-10}$; Wilcoxon rank-sum]. There was no significant difference between running and resting mice, as opposed to the small but significant difference in eye-movement and eye-movements free trials ($p = 0.49$ and $p = 0.0047$, respectively; Wilcoxon rank-sum). NS, not significant; **, $p < 0.005$; ***, $p < 0.0005$.

538 **Figure 2** Adaptation is modulated by stimulus relevance in awake mice. **(a)** Schematic of the
539 behavioral task. For the grating-irrelevant condition, movement of a virtual tunnel projected on a
540 toroidal screen was coupled to the locomotion (rotation and running on a spherical treadmill) of
541 the head-restrained mice (Dombeck et al. 2007). Mice were trained to orient and run to the end
542 of the tunnel for a water reward. We presented a horizontal sinusoidal moving grating in a
543 circular probe patch centered on the retinotopic location of the recording site, interspersed with
544 random intervals of gray (10-20 s; **Video 1**). **(b)** First and last paths of a sample mouse. The
545 colors show individual trials. **(c)** Task difficulty (length of the tunnel) was increased over
546 learning to keep the number of rewards approximately constant. **(d)** Learning curve of an
547 example mouse (solid line: exponential fit). The performance is quantified as fraction of time
548 spent running in the direction of the goal (±25°). **(e)** Data from animals trained in the behavioral
549 task under grating-irrelevant conditions. Traces show averaged calcium responses (GCaMP6f)
550 (Chen et al. 2013) of tuned putative excitatory cells to a moving sinusoidal grating. Curves
551 plotted as mean ± SEM (shading). **(f)** Same as **e** but for animals exposed to the grating-relevant
552 condition. For this condition, the visual stimulus on the screen was a replay of the visual flow
553 from one of the mice in the grating-irrelevant group. To match the initial responses of the
554 grating-relevant and the grating-irrelevant traces, ten percent of neurons were excluded from
555 analysis (see Materials and methods). Note that this did not change the results. **(g)** Slopes of
556 adaptation of the same cells as in **e** and **f** (line fit to the data in time window 1-10 s). In the
557 grating-irrelevant condition, the slope significantly decreases from the first to the following
558 sessions, as opposed to the grating-relevant condition (putative excitatory: 332 and 303 cells,
559 respectively; $p = 0.017$ and $p = 0.28$, respectively; Wilcoxon signed-rank). The slopes for the two
560 conditions are similar during the first session, but significantly differ during later sessions

(putative excitatory: 332 and 303 cells; $p = 0.84$ and $p = 0.0036$, respectively; Wilcoxon rank-sum). The solid curves are exponential fits to the data. Error bars represent mean ± SEM. **(h)** Same as **g** but for mean response to the grating. In the grating-irrelevant condition, the mean response significantly decreases from the first to the following sessions, as opposed to the grating-relevant condition (putative excitatory: 332 and 303 cells, respectively; $p < 10^{-4}$ and $p = 0.85$, respectively; Wilcoxon signed-rank). The mean responses for the two conditions are similar during the first session, but significantly differ during later sessions (putative excitatory: 332 and 303 cells; $p = 0.61$ and $p = 0.0015$, respectively; Wilcoxon rank-sum). NS, not significant; *, $p < 0.05$; **, $p < 0.005$; ***, $p < 0.0005$.

570 **Video 1** Sample mouse under grating-irrelevant condition in session 4.

**Figure 1-figure supplement 1** Adaptation in visual cortex of anesthetized mice is prevented by optogenetic silencing of cortical neurons (see also King et al. 2016). Neural activity was recorded with multi-tetrode arrays in anesthetized mice that express channelrhodopsin-2 (ChR2) in parvalbumin-positive (PV+) neurons. To test whether adaptation in V1 depends on local cortical activity, we presented a sustained moving grating with or without locally silencing the visual cortex and probed the V1 activity level immediately after the manipulation time window. **(a)** Averaged and binned (bin size 333 ms) spike responses of tuned putative excitatory cells to a moving square-wave grating at 100% contrast in anesthetized mice. The responses for three stimulus conditions are shown: Adapted, grating presented for 7 s; Control, grey screen presented for 3.5 s followed by 3.5 s of grating; LED+adapted, grating presented for 7 s with simultaneous optogenetic activation of PV+ cells during the first 3.5 s followed by a 0.5 s decrease of the optogenetic activation of PV+ cells (see Materials and methods). LED (optogenetic activation) and visual stimulus timings are illustrated by the top traces and marked by the vertical solid lines. The vertical dotted line indicates the time bin (first bin after LED off) used to compare the state of adaptation of the three stimulus conditions in **b**. Average traces are plotted as mean ± SEM (shading). **(b)** Averaged spike rate for the three stimulus conditions for the bins indicated by the vertical dashed lines in **a**. The LED+adapted condition evokes similar spike rates compared to the control and significantly more than the adapted condition (tuned putative excitatory: 109 cells; LED+adapted/adapted: $p < 10^{-10}$; LED+adapted/control: $p = 0.13$; adapted/control: $p < 10^{-10}$; Wilcoxon signed-rank). Bars plotted as mean ± SEM. **(c)** Same as **a** but for PV+ cells. **(d)** Same as **b** but for PV+ neurons. All conditions evoke similar spike rates (tuned PV+: 27 cells; LED+adapted/adapted: $p = 0.73$; LED+adapted/control: $p = 0.067$; adapted/control: $p = 0.17$; Wilcoxon signed-rank). **(e)** Scatterplot of the average spike rate

responses of all cells during the first 3.5 s of their preferred grating stimulus, with and without optogenetic stimulation of PV+ cells. Cells that increased their firing during the optogenetic stimulation of PV+ cells were classified as PV+ neurons, the remaining ones as putative excitatory cells. Highlighted cells (1-3) are shown in **f-h**. **(f)** Same as **a** but for a single cell classified as PV+. **(g,h)** Same as **f** but for two example cells classified as putative excitatory. NS, not significant; ***, $p < 0.0005$.

**Figure 1-figure supplement 2** Differences in contrast adaptation across cell-types can be revealed using two-photon imaging. PV+ neurons adapted less than putative excitatory cells, consistent with the idea that they might inhibit other neurons to produce contrast adaptation (A. J. Keller and Martin 2015). Moreover, iso- and cross-orientation adaptation had similar effects on the population (see also Stroud, Ledue, and Crowder 2012). In mouse V1, PV+ neurons are much less selective to a grating of different orientations than excitatory neurons (Atallah et al. 2012; Hofer et al. 2011; Kerlin et al. 2010). Therefore, an adaptation mechanism based on PV+ neurons would result in adaptation that is only weakly dependent on the orientation of the stimulus. Indeed, adapting putative excitatory cells to their preferred or null (orthogonal to preferred) orientation results in a significant, but small difference in adapted firing rates. Moreover, no difference was found when adapting PV+ cells with either iso- or cross-orientation (with respect to test orientation). **(a)** Neural activity was recorded with multi-tetrode arrays in anesthetized mice (same cells as in **Figure 1-figure supplement 1a,b**). Averaged and normalized responses of tuned putative excitatory and PV+ cells to a moving square-wave grating at 100% contrast presented for 7 s in anesthetized mice. Curves plotted as mean ± SEM (shading). **(b)** Adaptation is quantified as the mean decrease in normalized spike rate per second during the stimulus presentation (tuned putative excitatory: 109 cells; PV+: 27 cells; $p = 0.010$; Wilcoxon rank-sum). Bars plotted as mean ± SEM. **(c)** Neural activity of tuned putative excitatory compared to PV+ cells recorded with two-photon calcium imaging. Averaged and normalized calcium responses to a moving sinusoidal grating at 50% contrast presented for 7 s in anesthetized mice. Curves plotted as mean ± SEM (shading). **(d)** Adaptation is quantified as the mean decrease in normalized $\Delta F/F$ per second during the stimulus presentation (tuned putative excitatory: 545 cells; PV+: 78 cells; $p = 3.7 \times 10^{-4}$; Wilcoxon rank-sum). The initial rise was

excluded in the estimation of the slope (see Materials and methods). **(e)** Averaged responses of tuned putative excitatory cells in anesthetized mice to a moving sinusoidal grating at 50% contrast presented for 10 s followed by 10 s of a second stimulus of increased (100% contrast; dark traces) or decreased contrast (25% contrast; light traces). The first stimulus was either presented at the optimal (solid traces) or the orthogonal orientation of the neurons (dotted traces). The second stimulus was always presented at the optimal orientation. The two vertical dotted lines indicate the time window which was used to compare iso- and cross-orientation adaptation in **f**. ΔF/F traces plotted as mean ± SEM (shading). **(f)** Iso-orientation compared to cross-orientation adaptation (50% contrast) of tuned putative excitatory cells measured at 25% or 100% contrast. This is quantified as average ΔF/F after adaptation (seconds 11-12; indicated by the vertical dotted lines in **e**; 299 cells; 25%: $p < 10^{-10}$; 100%: $p < 10^{-4}$; Wilcoxon signed-rank). **(g)** Same as **e** but for PV+ cells. **(h)** Same as **f** but for PV+ cells (40 cells; 25%: $p = 0.12$; 100%: $p = 0.98$; Wilcoxon signed-rank). **(i)** Same as **e** but in awake mice. Note that the absence of adaptation to the moving sinusoidal grating at 50% contrast (0-10 s) cannot be explained by a response ceiling since the cells increase their responses when increasing the contrast to 100% (at 10 s). **(j)** Same as **f** but in awake mice (239 cells; 25%: $p = 0.0082$; 100%: $p = 0.14$; Wilcoxon signed-rank). **(k)** Same as **i** but for PV+ cells. **(l)** Same as **j** but for PV+ cells (33 cells; 25%: $p = 0.0064$; 100%: $p = 0.20$; Wilcoxon signed-rank). Bars plotted as mean ± SEM. NS, not significant; *, $p < 0.05$; ***, $p < 0.0005$.

**Figure 1-figure supplement 3** Contrast adaptation in anesthetized compared to awake mice and **e**ffects of running and eye-movements on adaptation in awake mice. **(a)** Scatterplot showing slopes of adaptation of tuned putative excitatory cells recorded in anesthetized and awake mice (same cells as in **Figure 1c,d**; line fit to the data in time window 1-9.75 s). Seventeen cells not visible in plot as they lie outside of the axis shown - 13 above and 4 below the diagonal. Red cross shows mean ± SEM. **(b)** Averaged responses of tuned putative excitatory cells to a moving sinusoidal grating at 50% contrast presented for 10 s in awake running and resting mice. See also **Figure 1d**. Note that the number of cells for running (51 cells) is smaller than for the resting condition (169 cells) because not all cells were recorded in both conditions. Curves plotted as mean ± SEM (shading). **(c)** Same as **b** but for trials with eye movements and eye movement-free trials.

**Figure 1-figure supplement 4** A large fraction of neurons in awake mice were suppressed during the stimulus and decreased their activity below baseline. The group of cells that were suppressed showed a positive average response under anesthesia. Of the putative excitatory cells, fewer cells showed a decrease compared to PV+ cells. Moreover, the magnitude of the decrease was larger for PV+ cells compared to putative excitatory cells. **(a)** All putative excitatory cells recorded in awake mice divided into groups which increase or decrease their activity in response to a moving sinusoidal grating at 50% contrast. The responses of the same groups of neurons are shown for the anesthetized mice. Note that the cells that are suppressed by the grating stimulation in awake mice are excited in anesthetized mice. The two vertical dotted lines indicate the time window which was used to compare the decrease in activity in **c**. Curves plotted as mean ± SEM (shading). **(b)** Same as **a** but for PV+ cells. **(c)** Cumulative density of cells based on their average activity in response to the grating. **(d)** Fraction of putative excitatory and PV+ cells in awake and anesthetized mice with a negative average $\Delta F/F$ (compared to baseline) in response to the grating. **(e)** Average decrease from baseline (of decreasing cells) in response to the grating (average of 8.75-9.75 s as indicated by the vertical dotted lines in **a,b**). Decreases are significantly larger in awake mice compared to anesthetized mice (putative excitatory awake: 208 cells; putative excitatory anesthetized: 99 cells; $p = 0.011$; PV+ awake: 28 cells; PV+ anesthetized: 9 cells; $p = 0.010$; Wilcoxon rank-sum). In awake mice, the decrease is significantly larger in PV+ compared to putative excitatory cells (putative excitatory: 208 cells; PV+: 28 cells; $p = 0.0038$; Wilcoxon rank-sum). *, $p < 0.05$; **, $p < 0.005$.

673 **Figure 2-figure supplement 1** Scatterplots showing slopes of adaptation of the cells in training
674 session 1 compared to the average slope in sessions 2-5 in awake mice (see also **Figure 2**; line fit
675 to the data in time window 1-10 s). **(a)** Grating-irrelevant condition (same cells as in **Figure**
676 **2e,g**; 28 cells not visible in plot as they lie outside of the axis shown, 16 above and 12 below the
677 diagonal). Red cross shows mean ± SEM. **(b)** Grating-relevant condition (same cells as in **Figure**
678 **2f,g**; 12 cells not visible in plot as they lie outside of the axis shown, 3 above and 9 below the
679 diagonal). Red cross shows mean ± SEM.

**Figure 2-figure supplement 2** Licking, running, and eye-movement behavior in awake mice. **(a-c)** Lick frequency for grating-relevant condition. **(a)** Baseline subtracted lick frequency of the two animals showing a significant increase in anticipatory licking from session 1 (dotted colored lines) to session 5 (solid colored lines). The two vertical dotted lines indicate the stimulus presentation and the vertical solid line at 0 s indicates the water reward. Inset: Average anticipatory lick frequency (-0.5 – 0 s) is significantly higher in session 5 compared to session 1 in these two animals (session 1: 111 trials, session 5: 144 trials, $p < 10^{-4}$ and session 1: 146 trials, session 5: 143 trials, $p < 10^{-10}$; Wilcoxon rank-sum). **(b)** Same as **a**, but for the animals with no significant increase in anticipatory licking (session 1: 145 trials, session 5: 144 trials, $p = 0.093$; session 1: 108 trials, session 5: 131 trials, $p = 0.083$; session 1: 108 trials, session 5: 135 trials, $p = 0.20$ and session 1: 144 trials, session 5: 135 trials, $p = 0.49$; Wilcoxon rank-sum). **(c)** Average pre-reward lick frequency (-0.5 - 0s) for all animals over all sessions. **(d)** Averaged responses of tuned excitatory cells of the same animals as in **a**, to a moving sinusoidal grating (displayed in the probe patch) for sessions 1 and 5. Ten percent of the neurons were excluded to match the initial conditions of the grating-relevant traces to the grating-irrelevant traces (see Materials and methods for details). Note that this did not change the results. Curves plotted as mean ± SEM (shading). **(e)** Averaged responses of tuned excitatory cells of the same animals as in **b**, to a moving sinusoidal grating (displayed in the probe patch) for sessions 1 and 5. Ten percent of the neurons were excluded to match the initial conditions of the grating-relevant traces to the grating-irrelevant traces (see Materials and methods for details). Note that this did not change the results. Curves plotted as mean ± SEM (shading). **(f)** Traces show the differences in averaged responses of tuned excitatory cells between session 1 and 5 for the three conditions: grating-irrelevant; grating-relevant without anticipatory licking; and grating-relevant with anticipatory

licking. **(g)** Slopes of adaptation of the same cells as in **d** and **e** are shown. For reward anticipating mice, the slope significantly increases from the first to the following sessions (putative excitatory: 77 cells; $p = 0.0022$; Wilcoxon signed-rank). For the non-anticipating mice, the slope did not show any significant difference from the first to the following sessions (putative excitatory: 226 cells; $p = 0.45$; Wilcoxon signed-rank). The trials of each session were divided into four quarters. The vertical dashed lines separate the individual sessions. The solid curve is an exponential fit to the data. Error bars represent mean ± SEM. **(h)** Same as **g** but for mean response to the grating. For reward anticipating mice, the mean response significantly increases from the first to the following sessions (putative excitatory: 77 cells; $p = 0.020$; Wilcoxon signed-rank). For the non-anticipating mice, the mean response did not show any significant change from the first to the following sessions (putative excitatory: 226 cells; $p = 0. 23$; Wilcoxon signed-rank). **(i)** Bar plot shows the mean response difference (session 5 – session 1) for the three traces in **f**. Reward anticipating mice have a significantly larger response difference compared to mice under grating-relevant condition (77 cells and 332 cells, respectively; $p < 10^{-4}$; Wilcoxon rank-sum) or non-anticipating mice (77 cells and 226 cells, respectively; $p = 9.0 \times 10^{-4}$; Wilcoxon rank-sum). There is no significant difference between grating-irrelevant and non-anticipating mice (332 cells and 226 cells, respectively; $p = 0.13$; Wilcoxon rank-sum). **(j)** Proportion of time spent running over sessions for grating-irrelevant and grating-relevant conditions. The time spent running is not significantly different for the grating-irrelevant compared to the grating-relevant condition (7 and 6 mice; session 1: $p = 0.84$; session 2: $p = 0.18$; session 3: $p = 0.53$; session 4: $p = 0.45$; session 5: $p = 0.23$; Wilcoxon rank-sum). Curves plotted as mean ± SEM (shading). **(k)** Same as **j**, but for mean speed. The mean speed is not significantly different for the grating-irrelevant compared to the grating-relevant condition (7 and

6 mice; session 1: p = 0.84; session 2: p = 0.45; session 3: p = 0.95; session 4: p = 0.84; session 5: p = 0.29; Wilcoxon rank-sum). Curves plotted as mean ± SEM (shading). **(l)** Same as **j** but for saccade frequency. The saccade frequency is not significantly different for the grating-irrelevant compared to the grating-relevant condition (7 and 6 mice; session 1: p = 0.63; session 2: p = 0.84; session 3: p = 0.53; session 4: p = 0.45; session 5: p = 0.073; Wilcoxon rank-sum). Curves plotted as mean ± SEM (shading). NS, not significant; *, $p < 0.05$; **, $p < 0.005$; ***, $p < 0.0005$.

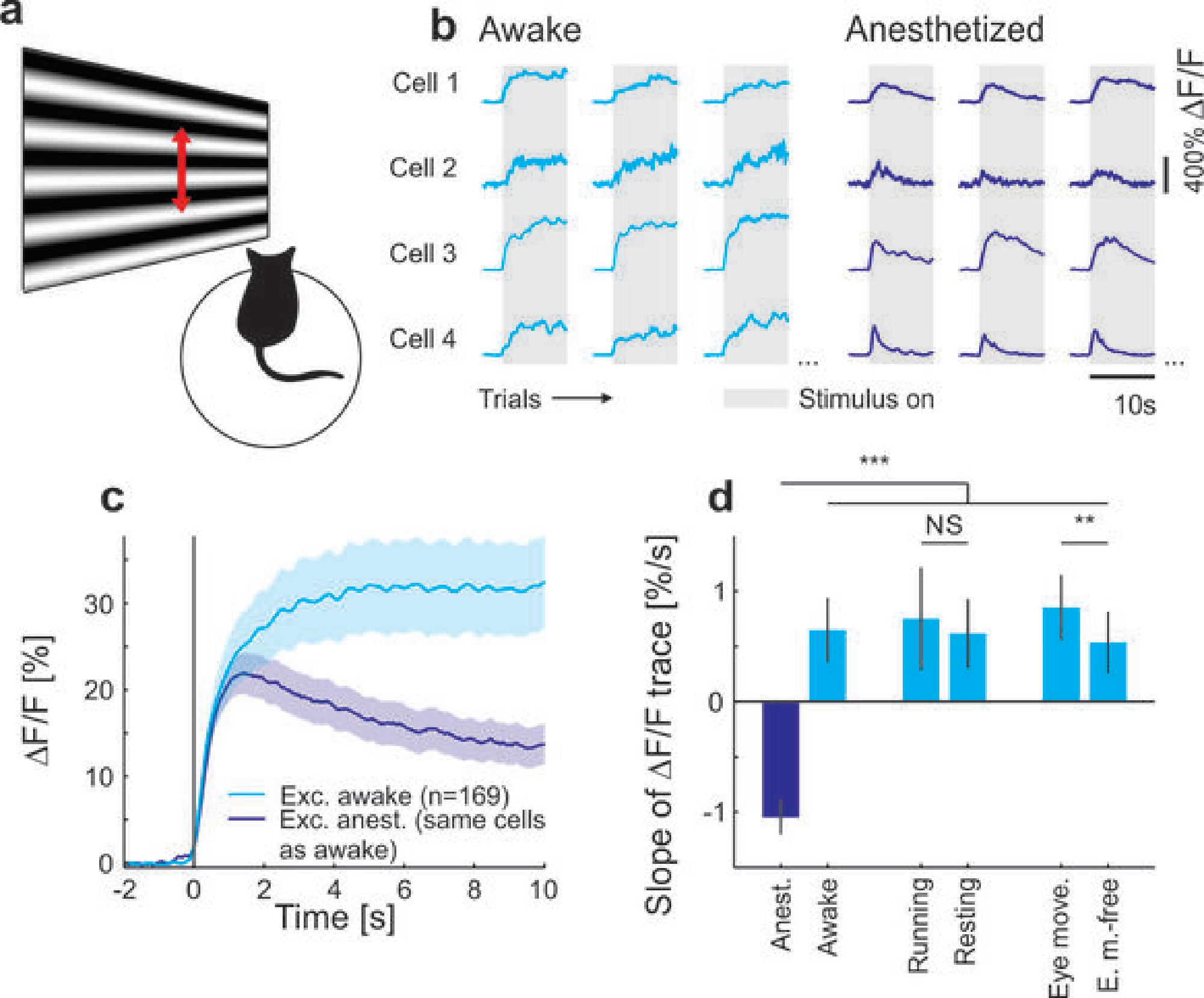
a
b
Awake
Anesthetized
Cell 1
Cell 2
Cell 3
Cell 4
400% ΔF/F
Trials
Stimulus on
10s
c
ΔF/F [%]
Time [s]
Exc. awake (n=169)
Exc. anest. (same cells as awake)
d
Slope of ΔF/F trace [%/s]
***
NS
**
Anest.
Awake
Running
Resting
Eye move.
E. m.-free

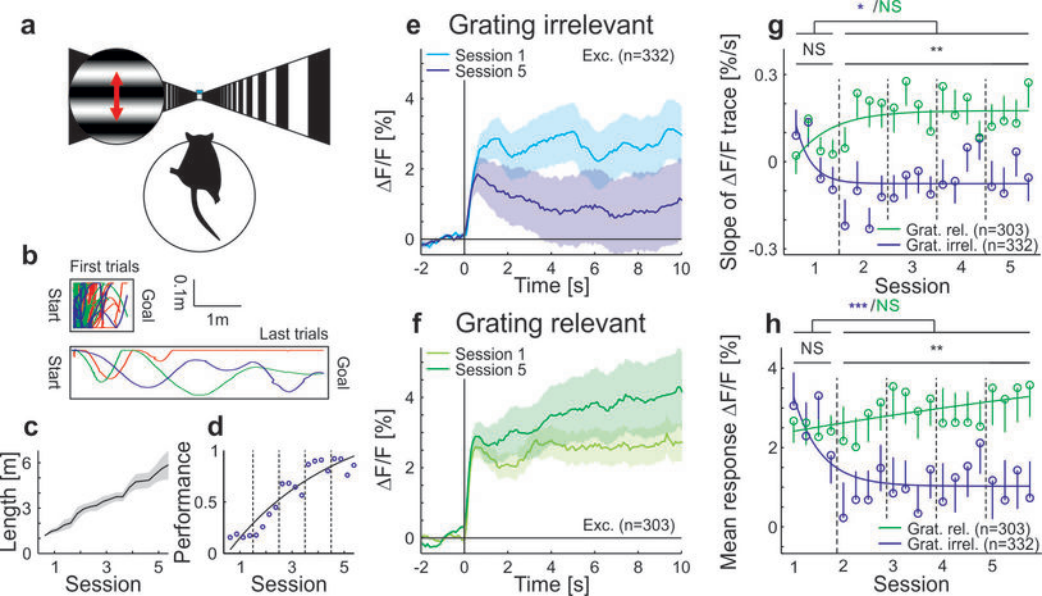
a
b
First trials
Start
Goal
0.1m
1m
Last trials
Start
Goal
c
Length [m]
Session
d
Performance
Session
e
Grating irrelevant
Session 1
Session 5
Exc. (n=332)
ΔF/F [%]
Time [s]
f
Grating relevant
Session 1
Session 5
Exc. (n=303)
ΔF/F [%]
Time [s]
g
* /NS
NS
**
Slope of ΔF/F trace [%/s]
Grat. rel. (n=303)
Grat. irrel. (n=332)
Session
h
***/NS
NS
**
Mean response ΔF/F [%]
Grat. rel. (n=303)
Grat. irrel. (n=332)
Session

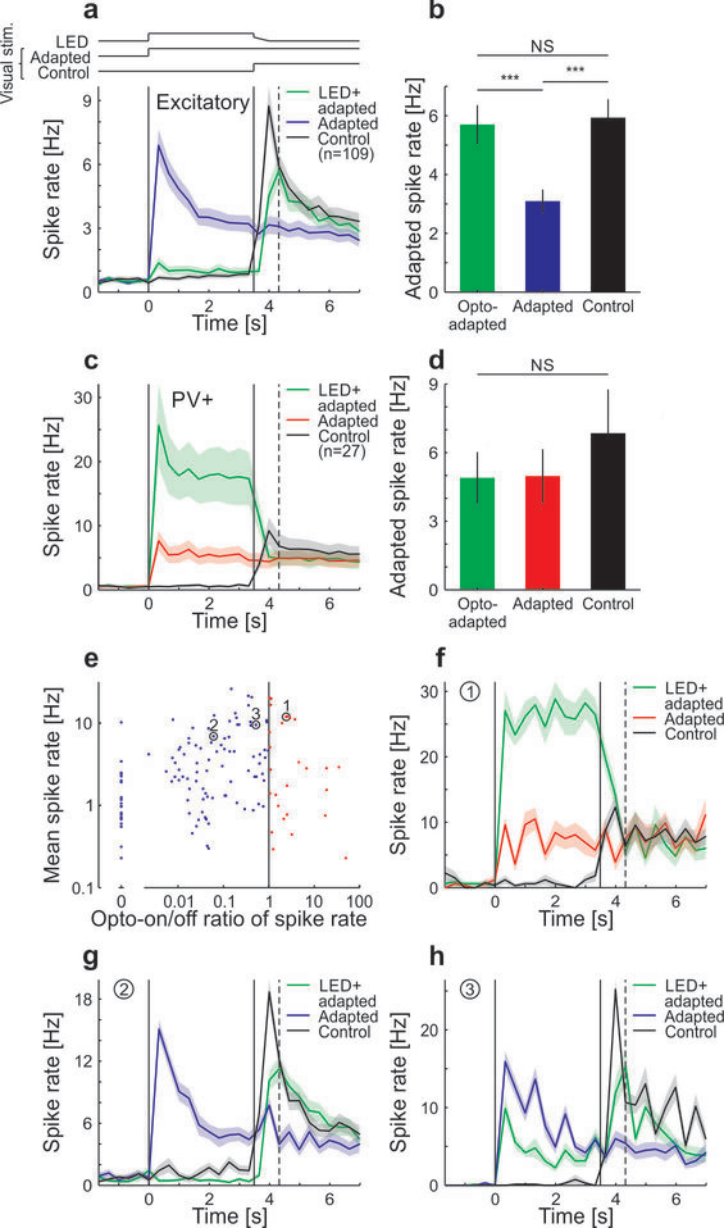
a
LED
Adapted
Control
Visual stim.
Excitatory
LED+ adapted
Adapted
Control (n=109)
Spike rate [Hz]
Time [s]
b
NS
***
***
Adapted spike rate [Hz]
Opto-adapted
Adapted
Control
c
PV+
LED+ adapted
Adapted
Control (n=27)
Spike rate [Hz]
Time [s]
d
NS
Adapted spike rate [Hz]
Opto-adapted
Adapted
Control
e
Mean spike rate [Hz]
Opto-on/off ratio of spike rate
f
①
LED+ adapted
Adapted
Control
Spike rate [Hz]
Time [s]
g
②
LED+ adapted
Adapted
Control
Spike rate [Hz]
Time [s]
h
③
LED+ adapted
Adapted
Control
Spike rate [Hz]
Time [s]

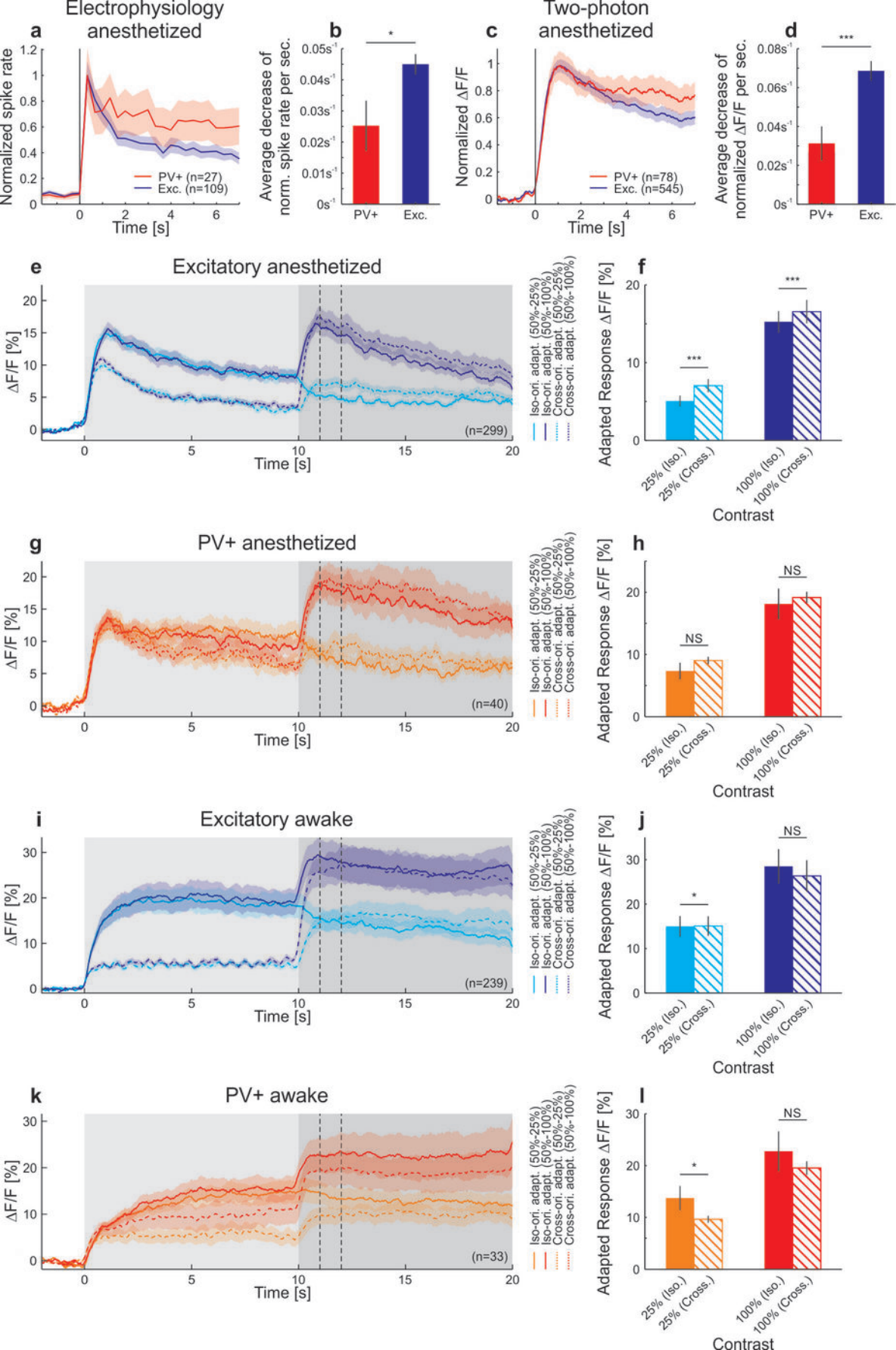
a
Electrophysiology
anesthetized
Normalized spike rate
PV+ (n=27)
Exc. (n=109)
Time [s]
b
Average decrease of
norm. spike rate per sec.
PV+
Exc.
c
Two-photon
anesthetized
Normalized ΔF/F
PV+ (n=78)
Exc. (n=545)
Time [s]
d
Average decrease of
normalized ΔF/F per sec.
PV+
Exc.
e
Excitatory anesthetized
ΔF/F [%]
(n=299)
Time [s]
Iso-ori. adapt. (50%-25%)
Iso-ori. adapt. (50%-100%)
Cross-ori. adapt. (50%-25%)
Cross-ori. adapt. (50%-100%)
f
Adapted Response ΔF/F [%]
25% (Iso.)
25% (Cross.)
100% (Iso.)
100% (Cross.)
Contrast
g
PV+ anesthetized
ΔF/F [%]
(n=40)
Time [s]
h
Adapted Response ΔF/F [%]
NS
Contrast
i
Excitatory awake
ΔF/F [%]
(n=239)
Time [s]
j
Adapted Response ΔF/F [%]
NS
Contrast
k
PV+ awake
ΔF/F [%]
(n=33)
Time [s]
l
Adapted Response ΔF/F [%]
NS
Contrast

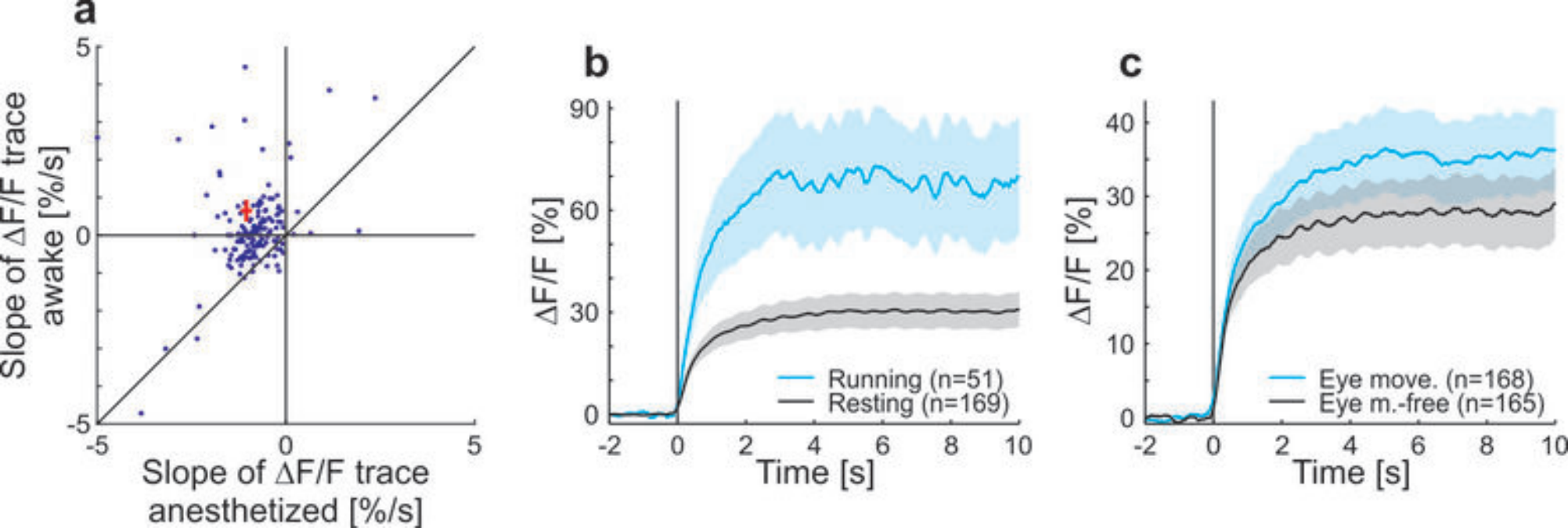
a
Slope of ΔF/F trace awake [%/s]
Slope of ΔF/F trace anesthetized [%/s]
5
0
-5
-5
0
5
b
ΔF/F [%]
90
60
30
0
-2
0
2
4
6
8
10
Time [s]
Running (n=51)
Resting (n=169)
c
ΔF/F [%]
40
30
20
10
0
-2
0
2
4
6
8
10
Time [s]
Eye move. (n=168)
Eye m.-free (n=165)

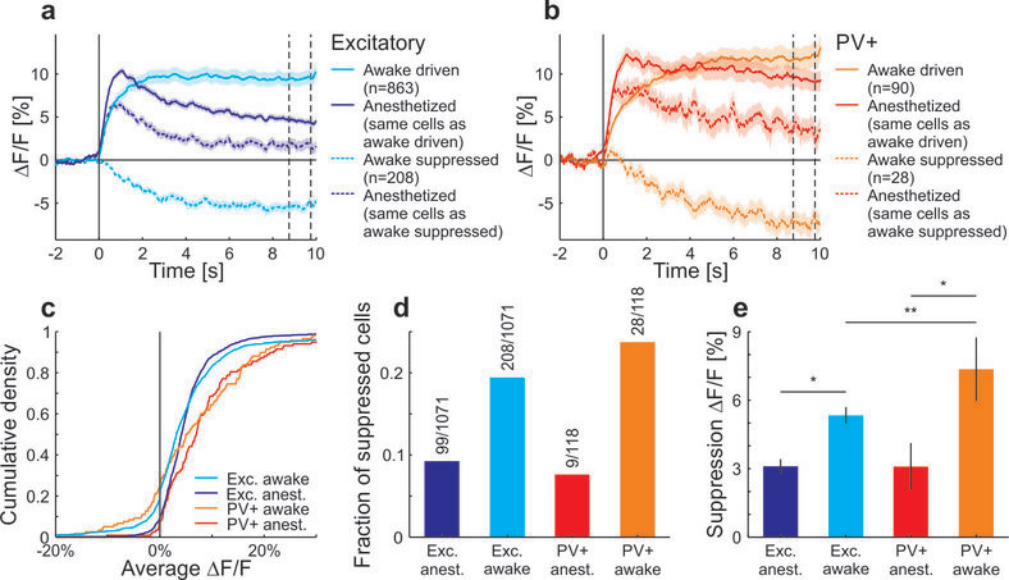
a
b
c
d
e
ΔF/F [%]
Time [s]
Excitatory
Awake driven (n=863)
Anesthetized (same cells as awake driven)
Awake suppressed (n=208)
Anesthetized (same cells as awake suppressed)
PV+
Awake driven (n=90)
Anesthetized (same cells as awake driven)
Awake suppressed (n=28)
Anesthetized (same cells as awake suppressed)
Cumulative density
Average ΔF/F
Exc. awake
Exc. anest.
PV+ awake
PV+ anest.
Fraction of suppressed cells
99/1071
208/1071
9/118
28/118
Exc. anest.
Exc. awake
PV+ anest.
PV+ awake
Suppression ΔF/F [%]

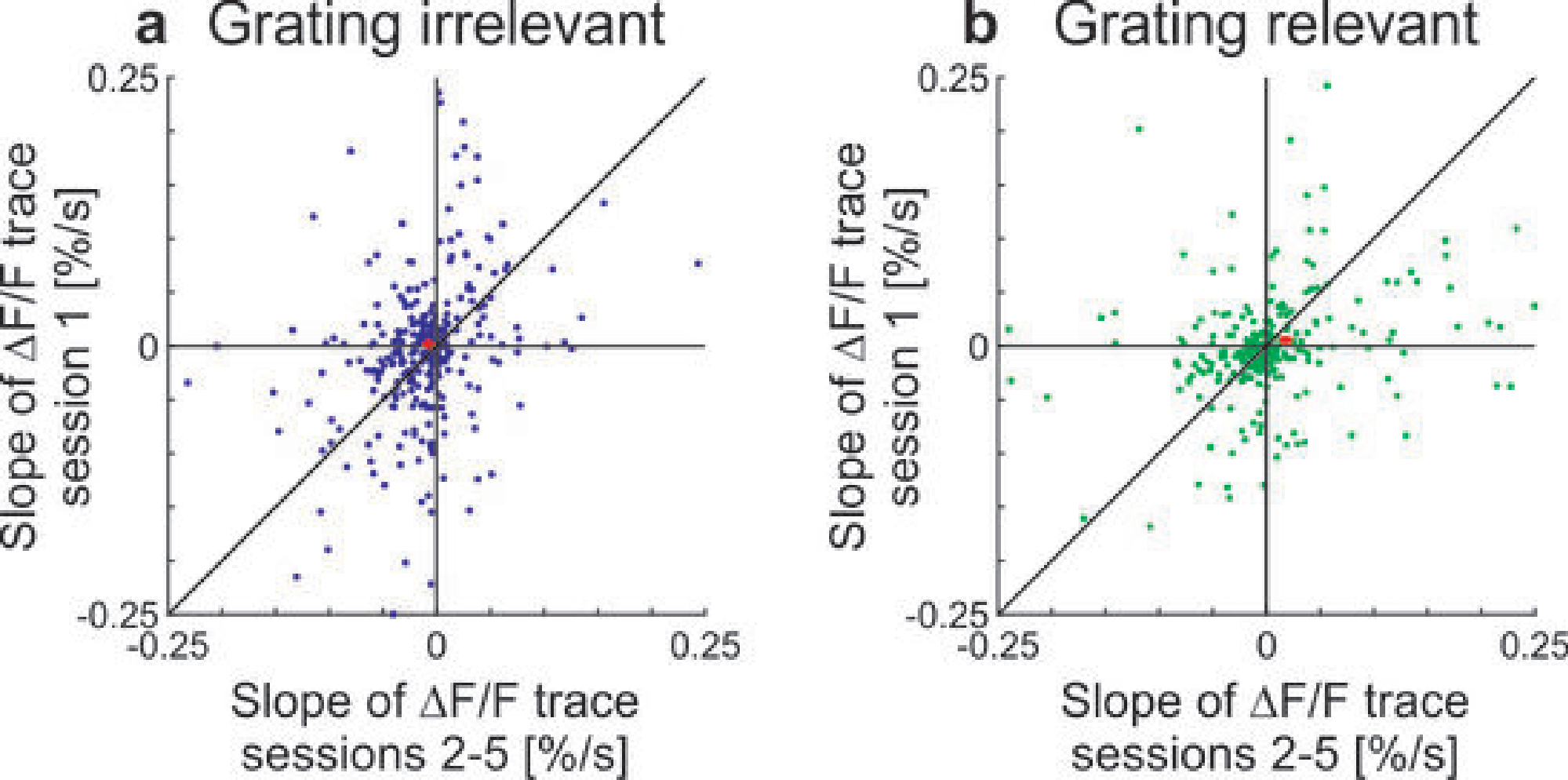
a Grating irrelevant
b Grating relevant
Slope of ΔF/F trace session 1 [%/s]
Slope of ΔF/F trace sessions 2-5 [%/s]
0.25
0
-0.25
-0.25
0
0.25

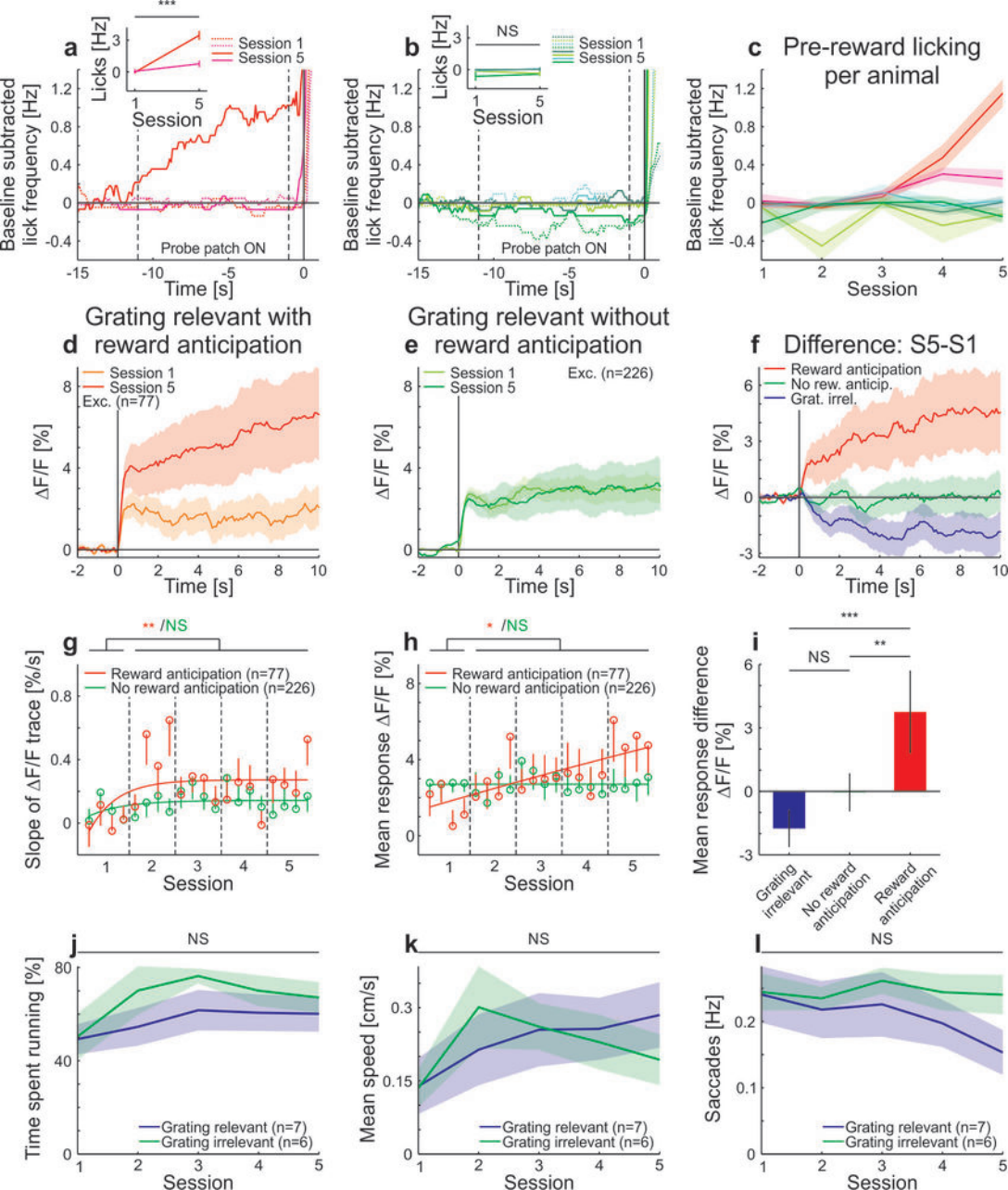
a
b
c
Pre-reward licking per animal
Licks [Hz]
Session
Session 1
Session 5
***
NS
Baseline subtracted lick frequency [Hz]
Probe patch ON
Time [s]
Session
d
Grating relevant with reward anticipation
e
Grating relevant without reward anticipation
f
Difference: S5-S1
Exc. (n=77)
Exc. (n=226)
Reward anticipation
No rew. anticip.
Grat. irrel.
ΔF/F [%]
Time [s]
g
h
i
** /NS
* /NS
Reward anticipation (n=77)
No reward anticipation (n=226)
Slope of ΔF/F trace [%/s]
Mean response ΔF/F [%]
Mean response difference ΔF/F [%]
Grating irrelevant
No reward anticipation
Reward anticipation
j
k
l
Time spent running [%]
Mean speed [cm/s]
Saccades [Hz]
Grating relevant (n=7)
Grating irrelevant (n=6)